

Commensurate-incommensurate phase transition in the presence of crystal deformation

K. Parlinski,* Y. Watanabe, K. Ohno, and Y. Kawazoe

*Institute for Materials Research, Tohoku University,
2-1-1 Katahira, Aoba-ku, Sendai 980, Japan*

(Received 9 June 1994)

A simple three-dimensional orthorhombic model of particles with displacive degrees of freedom interacting with the strain variables has been studied by the molecular-dynamics technique. The modulated degrees of freedom is coupled linearly to the shear and bilinearly to the bulk deformation component. The computer simulation has confirmed that the commensurate-incommensurate phase transition mechanism relies on nucleation and growth of stripples. Different configuration patterns of the initial commensurate phase revealed that the elastic domain walls between shear domains can be used to nucleate new discommensuration planes, and stripples are able to recover planar folding defects of the lattice, defects which are the result of heavy crystal deformation. It is shown that in the incommensurate phase the shear component forms a modulated field which follows the modulation wave with the same wave vector, but the bulk deformation component doubles the modulation wave vector.

I. INTRODUCTION

Some dielectrics¹ and metallic alloys^{2,3} exhibit incommensurate modulations. Usually such a modulated phase can be transformed to a commensurate one. Close to a phase transition point the incommensurate phase can be considered as an ordered sequence of domains of a reference commensurate phase separated by discommensuration planes. Typically, in the phase transition from commensurate to incommensurate phase a large number of discommensuration planes is generated in the crystal, and this process is carried on by the stripple mechanism.⁴⁻¹⁰ A stripple¹¹⁻¹⁴ resembles a disk built up from discommensuration planes and bordered by a deperiodization line. Stripples are nucleated by thermal fluctuations in the metastable states of usually overheated crystals, and later they grow, provided they exceed a critical size, similar to the classical nuclei in the first-order phase transition. However, in the first-order phase transition one nuclei is, in principle, able to transform the whole volume of the crystal. The peculiarity of the incommensurate phase is that one stripple adds to the system only one new modulation period, which usually means a few discommensuration planes. In the case of commensurate $k = 0$ to incommensurate phase transition each stripple carries on only two discommensuration planes. Thus, usually a vast number of stripples must be nucleated in order to complete the phase transition.

It is believed that the stripple mechanism of the commensurate-incommensurate phase transition can be perturbed by crystal imperfections, e.g., point defects, impurities,^{15,16} grain boundaries, dislocations, and surfaces of the crystal. Each of these imperfections can locally modify the potential and generate a stress field which in turn influences the incommensurate modulation.

The presence of random point defects enhances the hysteresis effects. Impurities may also serve as possible nucleation centers and can directly influence the properties of the modulated crystal. For example, systematic x-ray-diffraction measurements¹⁷ on mixed $(\text{Rb}_{1-x}\text{K}_x)_2\text{ZnCl}_4$ crystals show that point defects interact strongly with discommensuration planes, and act as pinning centers. The observation of memory effects shows that defects can also interact kinetically with modulation, by diffusing and relaxing in the "field" of the modulation.^{18,19} If the periodicity of this field is maintained constant for a sufficient long time, a defect density wave of the same periodicity as the ordering field develops, which acts as a periodicity "trap" with respect to all subsequent periodicity changes.

The properties of the modulated phase should also depend on the deformation and stress fields present in the crystal. These static fields arise from all types of defects including point defects, grain boundaries, dislocations, surfaces, and external stresses. There is experimental evidence for existence of such fields even in the free crystal. Namely, the phase transition between two commensurate phases, which is of first order, and should occur at one temperature, takes, as a rule, place during some temperature interval. One can attribute the coexistence interval of the two commensurate phases to the stress distributions present in the crystal, then from the phase boundary of the $p-T$ phase diagram one estimates the value of the stress dispersion, which for Rb_2ZnBr_4 (Ref. 20) and $[\text{N}(\text{CH}_3)_4]_2\text{ZnCl}_4$ (Ref. 21) is of the order of 300 bars.

The influence of the crystal stress and deformation on the modulation properties have not yet been studied. In this work we have undertaken a task to set up a simple orthorhombic model, which has a modulated phase and in which the modulation interacts linearly and bi-

linearly with the elastic deformation components. It is known that the effect of unit-cell deformation might cumulate over a long distance, therefore, strains are expected to play an essential role in the phase transitions involving long-wavelength modes,²² like in the commensurate $k = 0$ to incommensurate phase transition. The explicit treatment of strain allows one to consider an influence of elastic domain walls on the mechanism of the phase transition.

In Sec. II we describe the model, and the quantity which are calculated to define the action of the stripples. Some attention is devoted to the boundary conditions, which are essential for the simulations in the presence of strain variables. Section III describes the commensurate $k = 0$ to incommensurate phase transition obtained under different boundary and initial conditions for a system which is in a strengthened state and is confined to the restricted volume. The present simulations confirm the existence of stripple mechanism in all cases. It also shows that the coupled shear and deformation components follow the modulation waves, and that the elastic domain walls could serve as nuclei for discommensuration planes. They proved that the folding defects which were formed in the simulation to diminish heavy macroscopic

deformation of the simple crystallite could be removed by stripples, because the modulated phase consists of a regular sequence of elastic stripe domains which more easily accommodate large deformations.

II. MODEL

The model considered here is a simple three-dimensional orthorhombic lattice with one molecular object in the unit cell. Each object at the lattice site (i, j, k) has four degrees of freedom, three coordinates $X_{i,j,k}, Y_{i,j,k}, Z_{i,j,k}$, and a soft spin-like variable $S_{i,j,k}$, which describes the molecular orientation. Each molecular object interacts with its first and second neighbors via harmonic forces, and additionally, the soft spin is assumed to be in the anharmonic local potential. This potential can be treated as originating from molecular groups which are not explicitly taken into account in the model. The potential energy can be written as

$$V = V_{\text{local}} + V_{\text{intersite}} + V_{\text{elastic}} + V_{\text{coupling}}, \quad (1)$$

where

$$V_{\text{local}} = \sum_{i,j,k} [ES_{i,j,k}^2 + GS_{i,j,k}^4], \quad (2)$$

$$V_{\text{intersite}} = \sum_{i,j,k} [J_{1x}S_{i,j,k}S_{i+1,j,k} + J_{1y}S_{i,j,k}S_{i,j+1,k} + J_{1z}S_{i,j,k}S_{i,j,k+1} + J_{2z}S_{i,j,k}S_{i,j,k+2}], \quad (3)$$

$$V_{\text{elastic}} = \sum_{i,j,k} \left[A_x(R_{i,j,k;i+1,j,k} - a_0)^2 + A_y(R_{i,j,k;i,j+1,k} - b_0)^2 + A_z(R_{i,j,k;i,j,k+1} - c_0)^2 \right. \\ \left. + B_{xy}(R_{i,j,k;i+1,j\pm 1,k} - \sqrt{a_0^2 + b_0^2})^2 + B_{xz}(R_{i,j,k;i+1,j,k\pm 1} - \sqrt{a_0^2 + c_0^2})^2 \right. \\ \left. + B_{yz}(R_{i,j,k;i,j+1,k\pm 1} - \sqrt{b_0^2 + c_0^2})^2 \right], \quad (4)$$

$$V_{\text{coupling}} = \sum_{i,j,k} \left[-4A_z\alpha_z(R_{i,j,k;i,j,k\pm 1} - c_0)S_{i,j,k}^2 + 4B_{yz}\beta_{yz}(R_{i,j,k;i,j\pm 1,k\pm 1} - \sqrt{a_0^2 + c_0^2})S_{i,j,k} \right. \\ \left. - 4B_{yz}\beta_{yz}(R_{i,j,k;i,j\pm 1,k\mp 1} - \sqrt{a_0^2 + c_0^2})S_{i,j,k} \right], \quad (5)$$

where

$$R_{i,j,k;i',j',k'} = [(X_{i,j,k} - X_{i',j',k'})^2 + (Y_{i,j,k} - Y_{i',j',k'})^2 \\ + (Z_{i,j,k} - Z_{i',j',k'})^2]^{1/2}. \quad (6)$$

Here, a_0, b_0 , and c_0 denote the bare orthorhombic lattice constants. In the second and third terms of Eq. (5) either both upper or both lower signs of j and k increments should be taken. The soft-spin variable $S_{i,j,k}$ is defined in a spin subsystem, Eqs. (2) and (3), which itself is already able to form a modulated phase. Its harmonic part leads to a soft mode while its anharmonic fourth-order term stabilizes this mode. The modulation is directed along the Z axis. Such a model without a cou-

pling to strain has already been studied in one-,²³ two-,⁶ and three-dimensional⁷⁻¹⁰ cases. The harmonic part of the potential energy, Eqs. (2) and (3) can be transformed into a diagonal form, and then the corresponding eigenvector or dispersion curve reads

$$\omega^2(\mathbf{k}) = 2E + 2J_{1x} \cos 2\pi k_x a_0 + 2J_{1y} \cos 2\pi k_y b_0 \\ + 2J_{1z} \cos 2\pi k_z c_0 + 2J_{2z} \cos 4\pi k_z c_0, \quad (7)$$

where $\mathbf{k} = (k_x, k_y, k_z)$. Thus, the spin subsystem possesses a simple branch with a nonzero eigenvalue at the Brillouin zone center. When $\omega^2(\mathbf{k})$ becomes negative its minimum describes the wave vector and the direction of the static modulation. The extremum condition for the

minimum of $\omega^2(\mathbf{k})$ along the k_z direction relates the incommensurate wave vector $k_{z\min}$ of the modulation with the ratio of J_{1z}/J_{2z}

$$\cos 2\pi k_{z\min} c_0 = -\frac{J_{1z}}{J_{2z}}. \quad (8)$$

The two other nearest-neighbor parameters J_{1x} and J_{1y} define the curvature of the dispersion curve around the minimum in k_x and k_y directions, respectively.

A part of the ground state ($T = 0$) phase diagram for the spin subsystem defined by Eqs. (2) and (3) is shown in Fig. 1. It contains the normal phase (N), commensurate phases $0/1$ ($k = 0$), $1/6$, and $1/4$, and regions of incommensurate modulation. The computer simulations reported here have been carried out through the phase boundary from the commensurate $k = 0$ to the incommensurate phase. For that purpose the E and J_{1z} parameters were changed gradually. A similar phenomenon occurs in real crystals where the effective potential energy of these degrees of freedom, which forms the modulation pattern, is modified due to, for example, temperature changes.

The elastic potential energy consists of harmonic springs which are assumed to be related to both the nearest and next-nearest neighbors. This is the minimum range of elastic interaction which guarantees stability of the crystal lattice. Such a choice of forces assures as well that the phonon normal modes form three acoustic branches and hence the structure behaves correctly like an elastic medium.

The coupling energy, Eq. (5), between the elastic and spin subsystems consists of linear spin- YZ shear and bilinear spin- ZZ deformation terms. The linear term contributes to the phonon dispersion curves of the system. Its symmetry requires that along the $[0, 0, 1]$ direction the two branches which are of the same symmetry, namely the spin dispersion and the transfer acoustic phonon curves, cannot cross. As a result a combined phonon-spin

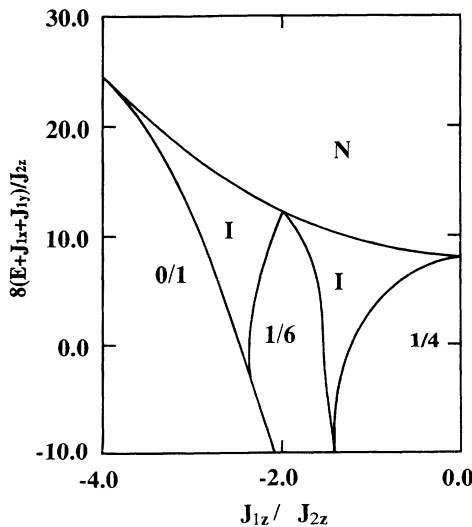


FIG. 1. Ground-state phase diagram of the soft-spin subsystem in the absence of the coupling potential energy, $V_{\text{coupling}} = 0$.

mode is formed. Therefore, this coupling is expected to play an important role in the long-wavelength limit where the elastic modes of the largest amplitudes could match the spin modes.

The bilinear term in the potential energy in Eq. (5), couples the square of the spin with the ZZ component of the deformation. Thus, any nonzero value of the spin $S_{i,j,k}$ involves elongation ($\alpha_z > 0$), or shortening ($\alpha_z < 0$) of the lattice constant in the Z direction. This bilinear coupling is allowed by symmetry for any value of the wave vector of the modulation.

The present model has been studied by the molecular-dynamics technique. The calculations have been performed on the Hitachi supercomputer S-3800/380, and graphics have been visualized by advanced visualization system implemented on the TITAN2 by Kubota Co. The simulated crystallite has a shape of rectangular parallelepiped and consists of either (A) $26 \times 26 \times 48 = 32448$ or (B) $38 \times 38 \times 76 = 109744$ unit cells. The Newtonian equations of motion have been solved by a simple difference scheme with the time step $\Delta t = 0.1\tau_0$, using the canonical ensemble with the temperature constant. The amplitude of average kinetic energy per degree of freedom is taken as the system temperature T . The boundary conditions are the crucial point for the simulation. Typically, either periodic or free surface boundary conditions are used. The first avoids dealing with the surface problem and forces all topological defects like stripples, to nucleate within the system. The second allows the topological defects to enter and leave the system through the surfaces. For elastic properties none of the above boundary conditions seem to be appropriate. The periodic boundary conditions would fix the volume of the simulated crystallite, and allow it to deform freely. Free boundary conditions would be too crude of an approximation for nonlarge linear sizes of the simulated crystallite, since elastic forces have long-range character. Therefore, we have used restricted volume boundary conditions,²⁴ i.e., the simulated crystallite was inserted into a cavity of fixed volume and fixed shape. Additionally, the magnitude of spins on the surfaces of the crystallite was set to be equal to the average spin amplitude. To avoid, at least partly, the surface problem, volume figures and maps presented below show only the inside of the simulated crystallite. For data analysis four layers of unit cells have been removed from each crystal surface.

To lower the effect of fluctuations a smoothed spin field $D_{i,j,k}$ was introduced as a spin average over a short time period ($1\tau_0$) and narrow space window. Thus,

$$D_{i,j,k} = g_0 \langle S_{i,j,k} \rangle + g_1 \langle S_{i,j,k\pm 1} \rangle + g_2 \langle S_{i,j,k\pm 2} \rangle, \quad (9)$$

where we have chosen g_0, g_1, g_2 to be 0.4, 0.2, 0.1, respectively. Thus, the following distributions (fields) have been used in describing the results: smoothed spin $D_{i,j,k}$, YZ shear $\sigma_{i,j,k}^{yz}$ and ZZ deformation $\sigma_{i,j,k}^{zz}$ components. The isosurfaces $D_{i,j,k} = 0$ of the three-dimensional spin field spanned over the simulated crystallite define the discommensuration planes.

The YZ component of the shear field was defined as

the angle between two vectors pointing towards Y and Z directions of the lattice, i.e.

$$\sigma_{i,j,k}^{yz} = - \left\langle \frac{\mathbf{R}_{i,j,k;i,j+1,k} \cdot \mathbf{R}_{i,j,k;i,j,k+1}}{|\mathbf{R}_{i,j,k;i,j+1,k}| |\mathbf{R}_{i,j,k;i,j,k+1}|} \right\rangle. \quad (10)$$

Positive and negative values of $\sigma_{i,j,k}^{yz}$ denote two elastic domains. The elastic domain walls will be oriented along the coherent matching planes which in this case are $(0, 1, 0)$ and $(0, 0, 1)$.

The ZZ component of the deformation field is equal to the deviation of the local lattice constant in the Z direction:

$$\sigma_{i,j,k}^{zz} = \left\langle \frac{(\mathbf{R}_{i,j,k;i,j,k+1} - c_0)}{c_0} \right\rangle. \quad (11)$$

Positive and negative values of $\sigma_{i,j,k}^{yz}$ denote local expansion and compression of the lattice, respectively. Both quantities $\sigma_{i,j,k}^{yz}$ and $\sigma_{i,j,k}^{zz}$ are averaged over a short time period ($1\tau_0$).

Some data will be presented in the form of two-dimensional maps in which the color of each pixel was set to the average values of given fields along the X direction, i.e., to $\frac{1}{N_0} \sum_{i=1}^{N_0} D_{i,j,k}$, $\frac{1}{N_0} \sum_{i=1}^{N_0} \sigma_{i,j,k}^{yz}$, or $\frac{1}{N_0} \sum_{i=1}^{N_0} \sigma_{i,j,k}^{zz}$. The following sequence of colors is used: blue (negative)-green-yellow-red (positive). Both the volume figures with isosurfaces and the color maps have been drawn on rect-

angular grids which have not been corrected for the crystal deformation.

III. ELASTIC DEFORMATION AND PHASE TRANSITION MECHANISMS

The mechanism of the commensurate $k = 0$ to incommensurate phase transition relies on nucleation and growth of stripples. The reported runs started from equilibrated particle configurations which corresponded to a commensurate phase $k = 0$ at finite temperature. Then, the potential parameters E and J_{1z} were gradually changed to the values which correspond to the stable incommensurate phase; see the phase diagram Fig. 1. Stripples or discommensuration planes appeared in the metastable state, and the place they occur and the manner in which they grow both depend on the spin-deformation coupling potential and the elastic domain pattern. In real incommensurate crystals the wave vector of the modulation shifts with varying temperature, pressure, or external field. This behavior is a consequence of a shift of the minimum of the soft mode $\omega^2(\mathbf{k})$ caused by the renormalization of the parameters of the effective potential energy by thermal fluctuations of degrees of freedom that otherwise are irrelevant for the incommensurate modulation. The computer simulation disregards the irrelevant degrees of freedom and mimics the above-mentioned behavior by simply changing the model parameters of the potential.

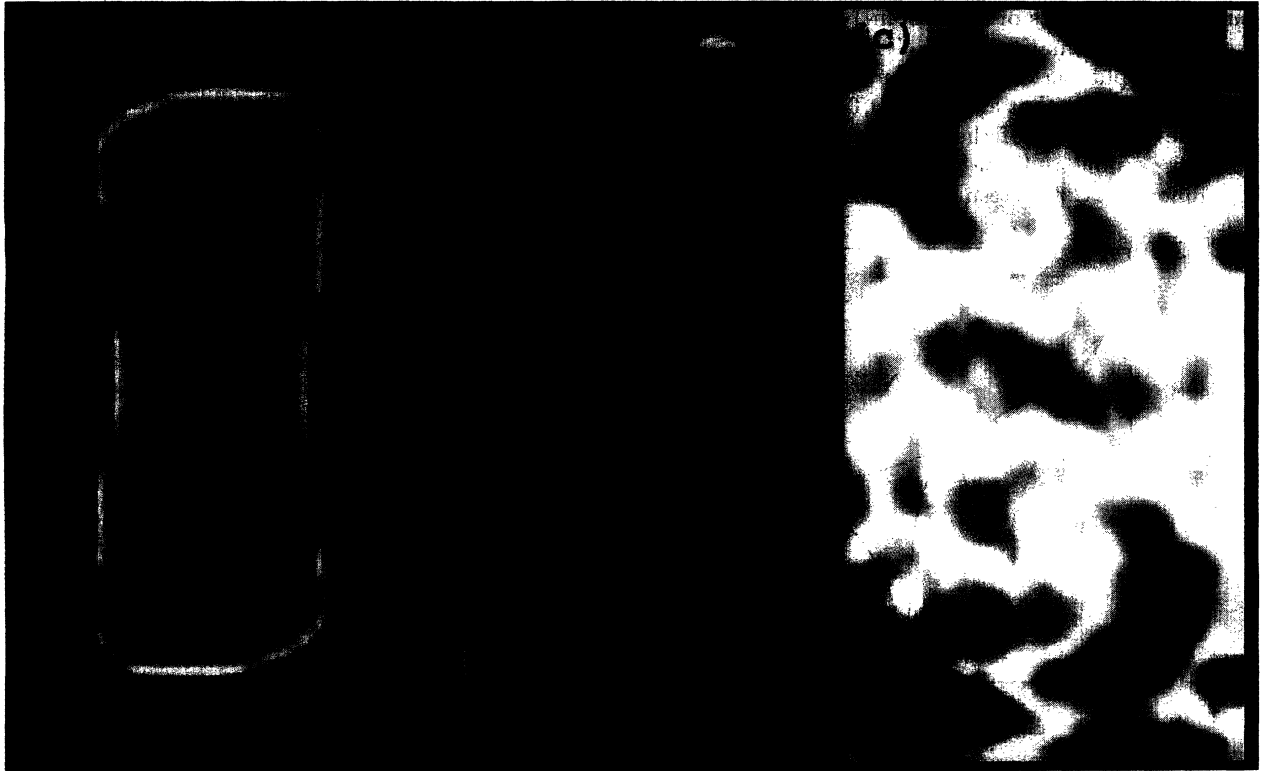


FIG. 2. The (a) smoothed spin, (b) YZ shear, and (c) ZZ deformation maps representing the initial particle configuration with the cylindrically shaped domain wall, before the commensurate $k = 0$ to incommensurate phase transition took place. The Y and Z axes point to horizontal and vertical directions, respectively.

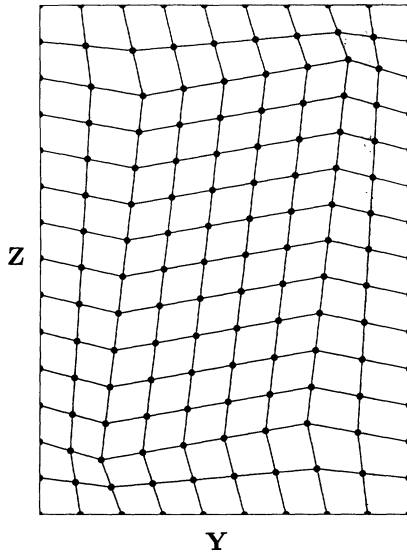


FIG. 3. The shear of the crystal lattice which contains cylindrically shaped elastic domain wall (schematically).

A. Expanded crystal with cylindrically shaped domain wall

The crystallite was confined to the restricted volume cavity of rectangular parallelepiped shape of size $26a_0 \times$

$26b_0 \times 48c_0$. The potential parameters were set to $A_x = 2.2$, $A_y = 1.8$, $A_z = 2.0$, $B_{xy} = 1.1$, $B_{xz} = 1.2$, $B_{yz} = 1.0$, $J_{1x} = -2.0$, $J_{1y} = -2.0$, $J_{1z} = -8.0$, $J_{2z} = 2.0$, $E = 9.0$, $G = 1.64$, and $\alpha_z = -0.41$, $\beta_{yz} = 0.41$, which involved small energy of anisotropy for the discommensuration planes, and hence rather easy disorientation of the discommensurations. The negative value of α_z requires that the equilibrium value of the lattice constant in the Z direction is less than c_0 . Moreover, a nonzero value of β_{yz} would cause a macroscopic YZ shear of the crystallite.

The initial configuration consisted of two domains. The positive spin domain was surrounded by its negative counterpart as shown in Figs. 2(a) and 4(a). The domain wall between them has the form of a deformed cylinder with symmetry axis directed along X . The elastic domain follows the spin pattern, Fig. 2(b). Such a domain shape reduces remarkably the macroscopic deformation of the crystallite inserted into the restricted volume, Fig. 3. Note that the elastic domain walls are oriented mainly along the coherent matching planes $[0, 1, 0]$ and $[0, 0, 1]$. Particularly high YZ shear deformation occurs in the upper-right and lower-left corners of the map, Fig. 2(b) (red spots). The ZZ deformation component is not sensitive to the domain wall changes. The map, Fig. 2(c), indicates, however, that an increased compression occurs at the upper-right and lower-left corners (blue spots) of the crystallite, and a somewhat smeared expan-



FIG. 4. Volume representation of the discommensuration planes (isosurface $D_{i,j,k} = 0$), showing four stages of the phase transition from commensurate $k = 0$ to incommensurate phase with initial domain pattern (a) in the form of a deformed cylinder. The particle configurations in (a) and (d) are the same as in the maps in Figs. 2 and 5, respectively. The X , Y , and Z axes point to vertical, out of the figure plane, and horizontal directions of the crystallite, respectively.

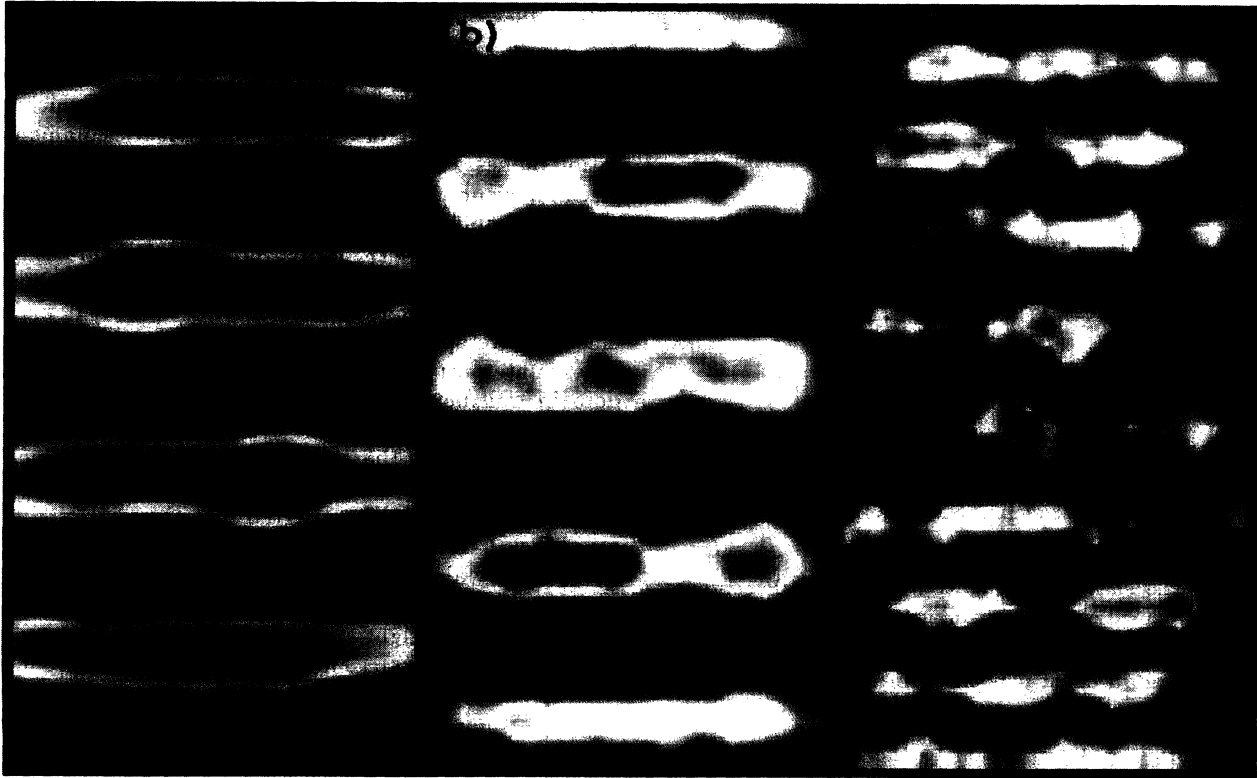


FIG. 5. The (a) smoothed spin, (b) YZ shear, and (c) ZZ deformation maps representing the final particle configuration after the phase transition from commensurate $k = 0$, with cylindrically shaped domain walls, to incommensurate phase took place. The Y and Z axes point to horizontal and vertical directions, respectively.

sion (red spots) close to the two remaining corners.

During the run the initial values of E and J_{1z} parameters have been changed up to the values 7.0 and -5.0 , respectively. These changes put the crystallite into the metastable conditions and the system reaction was such that parts of the domain walls, which were parallel to the modulation direction, started to wave, as is shown

in Fig. 4(b). The outer tips of this wave went to the crystal surface, where they split off and formed a discommensuration plane, Fig. 4(c). Later the remaining discommensurations followed the same way, Fig. 4(d).

The maps of the final incommensurate phase are shown in Fig. 5, where, of course, the modulation is formed by stripes of positive (red) and negative (blue) values of spin.

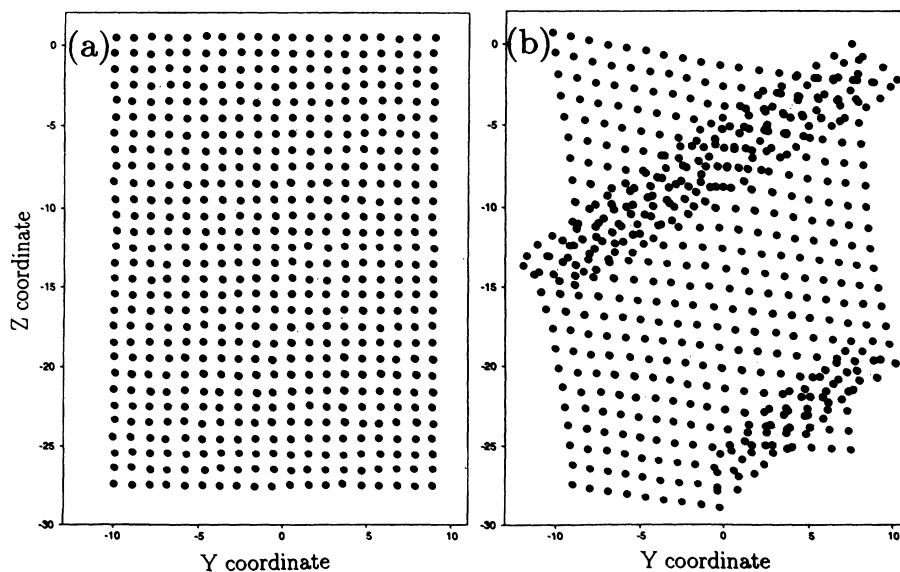


FIG. 6. Snapshot of particle positions in the middle layer of the crystallite for (a) expanded and (b) compressed crystal cases.

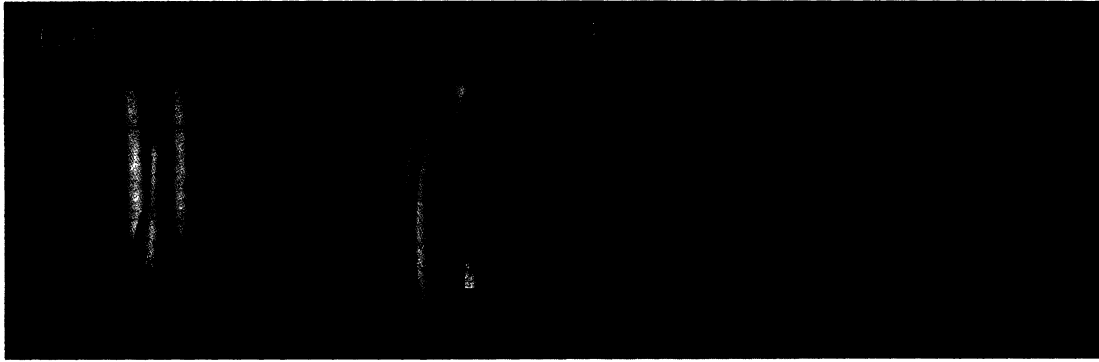


FIG. 7. Volume representation of the discommensuration planes (isosurface $D_{i,j,k} = 0$) taken (a) during phase transition from commensurate phase $k = 0$ to incommensurate phase, and (b) in the final incommensurate phase. The X , Y , and Z axes point to vertical, out of the figure plane, and horizontal directions of the crystallite, respectively.

Yellow lines denote small displacements and correspond to the discommensurations. The YZ shear component, Fig. 5(b), arranged as a sequence of elastic domains, and each elastic domain wall occur at the same place as the discommensuration. The ZZ deformation component, Fig. 5(c), shows a more random pattern, in which, however, it is possible to elucidate the doubling of the modulation wave vector. Indeed, the pattern of the “domain walls” in Fig. 5(c) seems to occur at twice as small a separation. That means that the characteristic modulation wave vector of the ZZ deformation field is twice as large than the one corresponding to the main modulation.

B. Expanded crystal

A similar run as described in Sec. III A for the expanded crystal with cylindrically shaped domain walls was made with the larger system B. The potential parameters for this run were generally twice as large than previously used and were set to $A_x = 4.4$, $A_y = 3.6$, $A_z = 4.0$, $B_{xy} = 2.2$, $B_{xz} = 2.4$, $B_{yz} = 2.0$, $J_{1x} = -4.0$, $J_{1y} = -4.0$, $J_{1z} = -16.0$, $J_{2z} = 4.0$, $E = 16.5$, $G = 2.35$, and $\alpha_z = -0.41$, $\beta_{yz} = 0.41$. The system was inserted into a restricted volume cavity of the size $38a_0 \times 38b_0 \times 76c_0$ with rectangular parallelepiped shape. The crystallite

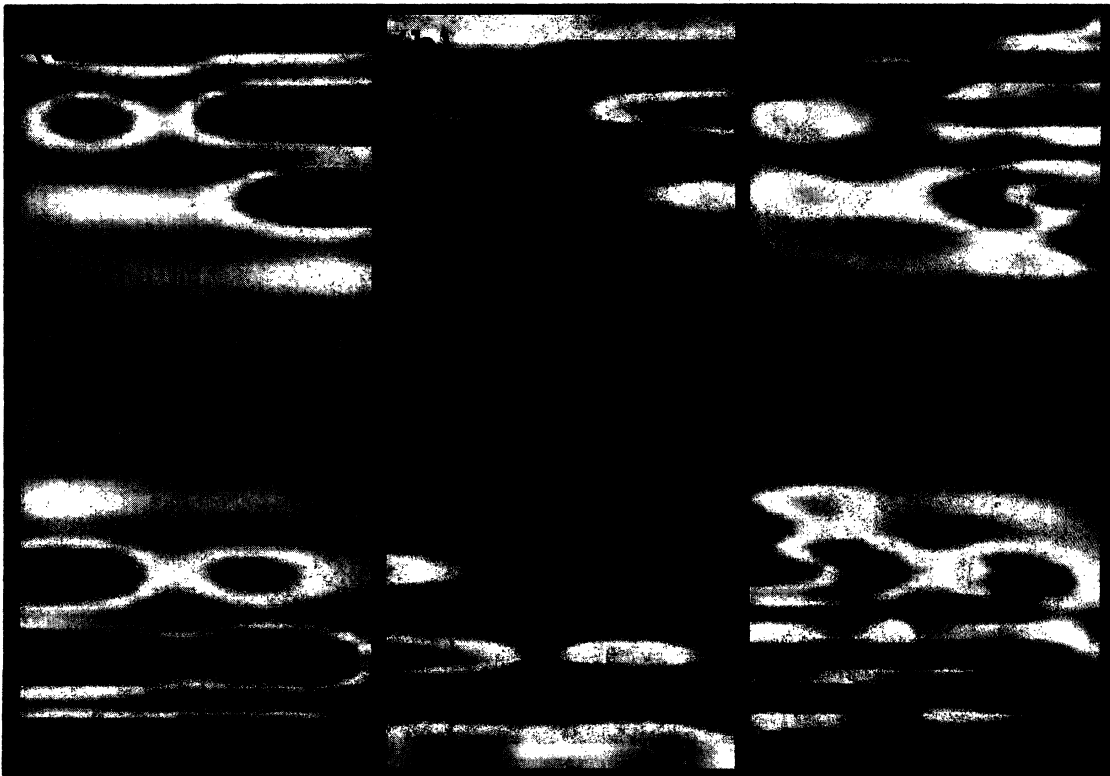


FIG. 8. The (a) smoothed spin, (b) YZ shear, and (c) ZZ deformation maps made during the phase transition from commensurate phase $k = 0$ to incommensurate phase. The particle configuration was the same as for Fig. 7(a). The Y and Z axes point to horizontal and vertical directions, respectively.

was uniformly expanded and remained in a strengthened, although in a single, domain state as shown in Fig. 6(a). During the run J_{1z} and E potential parameters were changed to values of -10.0 and 13.0 , respectively. In this way the crystallite went to a metastable state. The temperature of the run $T = 0.04$ was kept constant. Close to the end of the run stripples were nucleated mainly close to the opposite corners of the crystallite, Fig. 7(a), where the largest stresses occurred due to closing the crystal in the cavity. Each stripple produces two discommensuration planes. In Fig. 8 we show a smoothed spin, YZ shear, and ZZ deformation maps, which are the projection of the system on the YZ plane. The stripples (blue) as well as some stripes of the modulation are seen in Fig. 8(a). The YZ shear pattern, shown in Fig. 8(b) generally follows the soft-spin configuration. Thus, negative (blue) displacement of spin involves a positive YZ shear (red). The ZZ deformation component, Fig. 8(c), which is bilinearly coupled to the strain, has a tendency to double the modulation wave vector, so that the largest compression (blue) occurs just at the place of the maximum spin modulation amplitude. Moreover, one notices a ZZ expansion region (red) at the point of the deperiodization line of the stripples. There, the spin amplitude is close to zero, the α_z coupling term ceases to contribute, and the configuration becomes highly unstable, therefore, the lattice could be at this point considerably expanded.

C. Compressed crystal

In the case of compressed crystal the volume of the cavity was smaller than the volume required by the crystal with free boundary conditions. The potential parameters and the size and shape of cavity were the same as used for the expanded crystal in Sec. III B, with the only exception that the bilinear coupling coefficient was positive and was set to $\alpha_z = 0.2$. The macroscopic shape of the free crystallite could be sheared and elongated along the Z direction, in comparison with its size and shape in the absence of coupling ($\alpha_z = \beta_{yz} = 0$). Thus, it could either be compressed uniformly, or it could generate defects which are able to compensate the deformation. And indeed, the crystal, equilibrated in the commensurate $k = 0$ phase formed a type of planar defect shown in Fig. 9(a). A view of the corresponding particle configurations is given in Fig. 6(b). Unit cells between the planar defects remain in the perfect crystalline state, while those in the defect regions are heavily deformed. A closer look at the particle configurations reveals a folding of the crystal lattice in the defect region. The folds reduce both the macroscopic shear and the elongation of the crystallite. We have found that in this region 7% of nearest-neighbor pairs of particles fall below the distance 0.6 of the average lattice constant, and a few far-away lattice sites become nearest-neighbor. Unfortunately, the



FIG. 9. Volume representation of the YZ shear component (isosurface $\sigma_{i,j,k}^{yz} = 0$), showing four stages of the phase transition from commensurate $k = 0$ to incommensurate phase for the compressed crystal model. The same states of the crystallite are drawn in Fig. 11 for the discommensuration planes. The X , Y and Z axes point to vertical, out of the figure plane, and horizontal directions of the crystallite, respectively.

interaction between the newly arised nearest-neighbors pairs was not taken into account in the numerical code, since it would be required to update the neighboring list which due to our vectorization procedure must be kept constant.

In Fig. 10 the maps of smoothed spin, YZ shear, and ZZ deformation are shown in the initial states. Each fold consists of two edges seen in Fig. 10 as collection of dots with remarkably large deformation. The separation between subsequent folds as well as their orientation depend on the values of α_z and β_{yz} parameters. For twice as large α_z six folds appeared in the same crystallite.

To bring the system to the incommensurate phase the potential parameters were gradually changed to $E = 13.0$ and $J_{1z} = -10.0$. The temperature was kept constant at $T = 0.04$. Stripples were nucleated and they transformed the crystal to the incommensurate phase. Some stages of the evolution of YZ shear and of the discommensuration pattern are compared in Figs. 9 and 11, respectively. Figures 9(a) and 11(a) correspond to an initial commensurate domain with planar defects. The first stripple, shown in Fig. 11(b) appears also in the YZ shear field, Fig. 9(b). The stripples destroy the folds and recover completely the perfect crystal lattice. The final incommensurate modulation is accompanied by the sequence of shear elastic stripe domains characterized by the same incommensurate wave vector as the main modulation.

The stripe elastic domains are able to reduce the internal stresses in ZZ direction.

IV. FINAL REMARKS

The results of the simulations confirm the existence of the stripple mechanism also in the presence of deformation. The stripples have a structure determined by the domains of the reference commensurate phase $k = 0$. All simulations were carried out on a system inserted into a restricted volume and we believe that such conditions occur inside a macroscopic crystal. To be consistent with the approach and to model properly the deformations of the crystallite, we did not impose the periodic boundary conditions, instead, the spin component was set at the surface to a constant value. Even then one is not able to avoid the stripple nucleation at crystal edges and surfaces. Unfortunately, periodic boundary conditions could be imposed only on all degrees of freedom simultaneously. If one imposes periodic boundary conditions on the spin variable and leaves the surfaces free for the strain, a number of unphysical assumptions about a spin-strain coupling at the crystallite surfaces are required.

In this work we have explored only simple cases where the lattice was macroscopically deformed due to restricted volume. Then, it was proved that the elas-

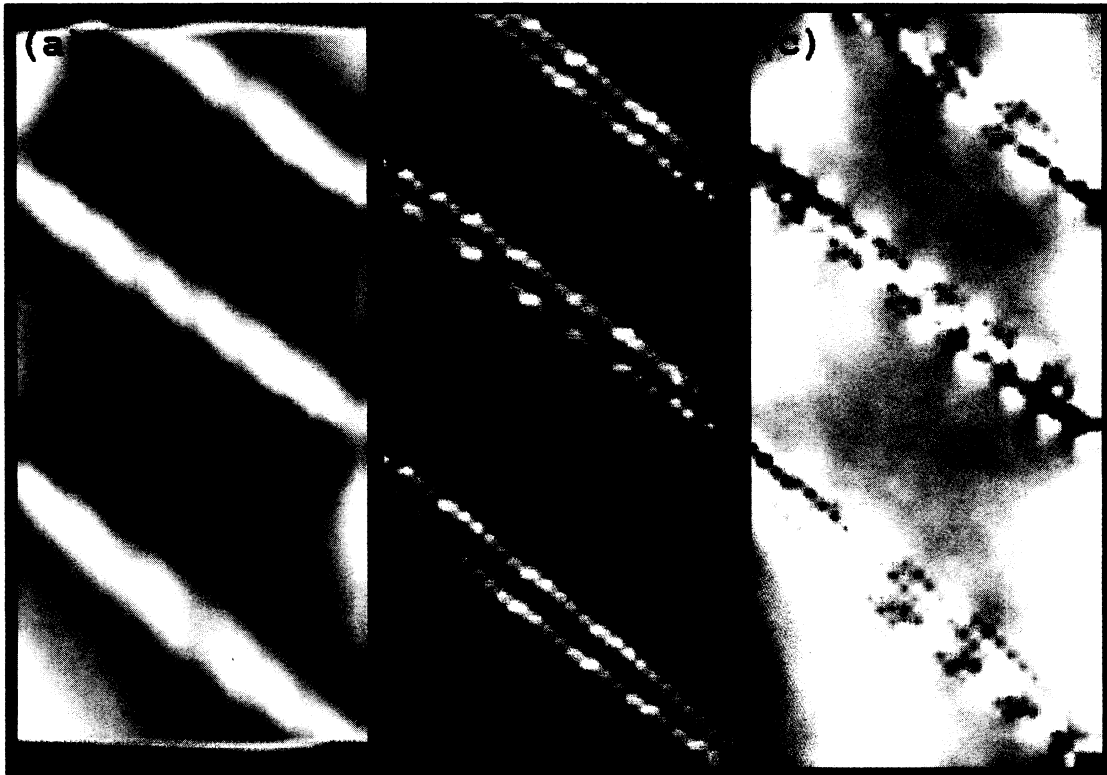


FIG. 10. The (a) smoothed spin, (b) YZ shear, and (c) ZZ deformation maps representing the initial particle configuration of the compressed crystal model before the commensurate $k = 0$ to incommensurate phase transition took place. The maps are drawn from the same state as the volume representations in Figs. 9(a) and 11(a). The Y and Z axes point to horizontal and vertical directions, respectively.

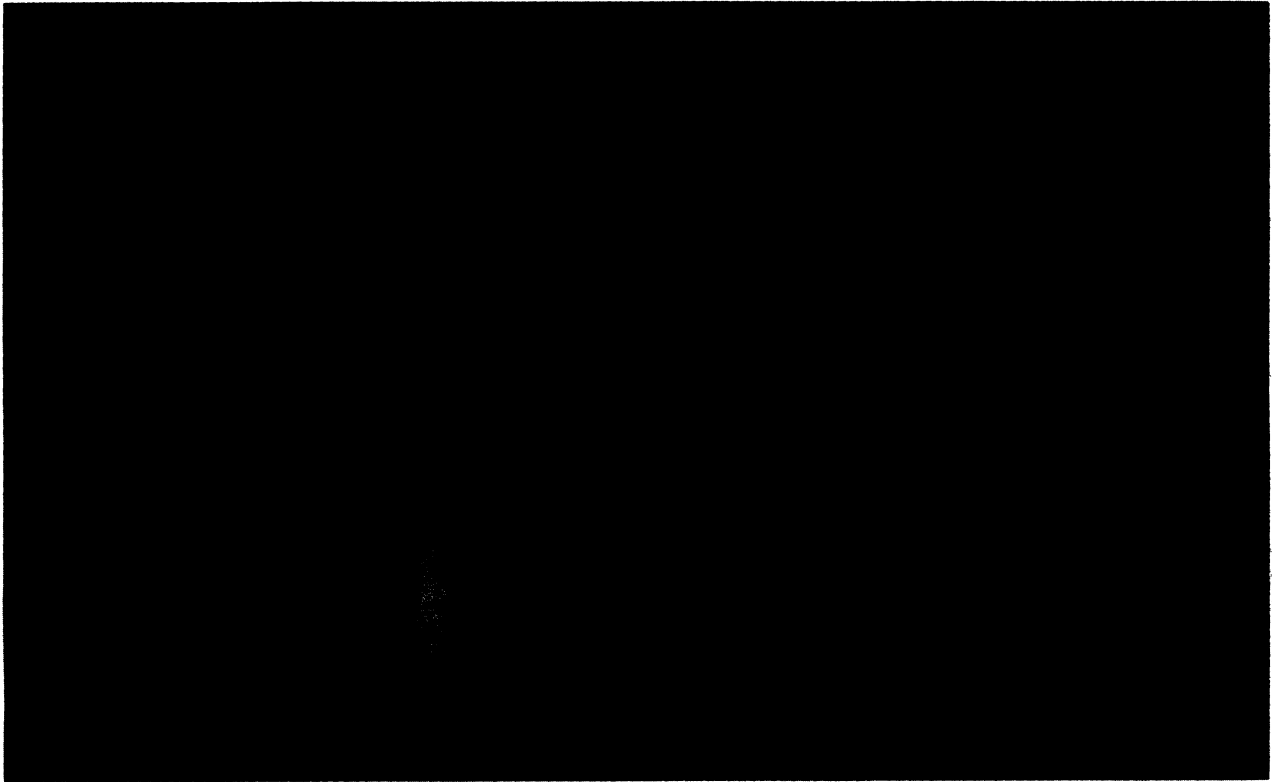


FIG. 11. Volume representation of the discommensuration planes (isosurface $D_{i,j,k} = 0$), showing four stages of the phase transition from commensurate $k = 0$ to incommensurate phase for the compressed crystal model. The X , Y and Z axes point to vertical, out of the figure plane, and horizontal directions of the crystallite, respectively.

tic domain walls which are oriented along the matching plane directions could be converted to discommensuration planes. Another effect found in this work is related to the recovering of heavily deformed lattice folds by stripples which redistribute the field of stresses and produce a configuration of tiny stripes of elastic domains, which are able, in turn, to accommodate larger deformations. In computer simulations these folds are rather unphysical objects, however, in real crystals, similar planar defects arise during plastic deformation. One hopes that an incommensurate phase would be able to recover these defects at least partly.

ACKNOWLEDGMENTS

The authors would like to thank M. Sluiter for many discussions and M. Ikeda for extensive help in handling the computer systems. One of us (K.P.) would like to express his thanks to the staff of the Laboratory of Materials Design by Computer Simulation, Institute of Materials Research, Tohoku University, for their great hospitality and assistance during his stay, and the Hitachi Corporation for financial support. This work was partially supported by the State Committee of Scientific Research (KBN), Grant No. 2 2377 92 03.

* On leave from the Institute of Nuclear Physics, ul. Radzikowskiego 152, 31-342 Cracow and Academic Computer Centre, Cyfronet, Cracow, Poland.

¹ H.Z. Cummins, Phys. Rep. **185**, 211 (1990).

² Y. Fujino, H. Sato, M. Hirabayashi, E. Aoyagi, and Y. Koyama, Phys. Rev. Lett. **58**, 1012 (1987).

³ G. van Tendeloo, J. van Landuyt, P. Delavignette, and S. Amelinckx, Phys. Status Solidi A **25**, 697 (1974).

⁴ H. Bestgen, Solid State Commun. **58**, 197 (1986).

⁵ H. Sakata, K. Hamano, X. Pan, and H.G. Unruh, J. Phys. Soc. Jpn. **59**, 1079 (1990).

⁶ K. Parlinski, Phys. Rev. B **35**, 8680 (1987).

⁷ K. Parlinski, Phys. Rev. B **39**, 12154 (1989).

⁸ K. Parlinski, Phys. Rev. B **48**, 3016 (1993).

⁹ K. Parlinski, F. Dénoyer, and G. Eckold, Phys. Rev. B **43**, 8411 (1991).

¹⁰ K. Parlinski and F. Dénoyer, Phys. Rev. B **41**, 11428 (1990).

¹¹ K.K. Fung, S. McKernan, J.W. Steeds, and J.A. Wilson, J. Phys. C **14**, 5417 (1981).

¹² V. Janovec, Phys. Lett. **99A**, 284 (1983).

¹³ K. Kawasaki and Y. Yamanaka, Phys. Rev. B **34**, 7986 (1987).

¹⁴ K. Parlinski, Comput. Phys. Rep. **8**, 153 (1988).

- ¹⁵ H.G. Unruh, *J. Phys. C* **16**, 3254 (1983).
- ¹⁶ J.P. Jamet and P. Lederer, *J. Phys. (Paris)* **44**, L257 (1983).
- ¹⁷ H. Mashiyama, S. Tanisaki, and K. Hamano, *J. Phys. Soc. Jpn.* **51**, 2538 (1982).
- ¹⁸ C.L. Folcia, J.M. Perez-Mato, and M.J. Tello, *Ferroelectrics* **79**, 275 (1988).
- ¹⁹ G. Errandonéa, *Phys. Rev. B* **33**, 6261 (1986).
- ²⁰ K. Parlinski, R. Currat, C. Vettier, I.P. Aleksandrova, and G. Eckold, *Phys. Rev. B* **46**, 106 (1992).
- ²¹ G. Eckold and K. Parlinski, *Physica B* **180&181**, 318 (1992).
- ²² V. Dvořák, V. Janovec, and Y. Ishibashi, *J. Phys. Soc. Jpn.* **52**, 2053 (1983).
- ²³ T. Janssen and J.A. Tjon, *Phys. Rev. B* **25**, 2245 (1981).
- ²⁴ A.L. Roytburd, *Phase Transitions* **4**, 1 (1993).

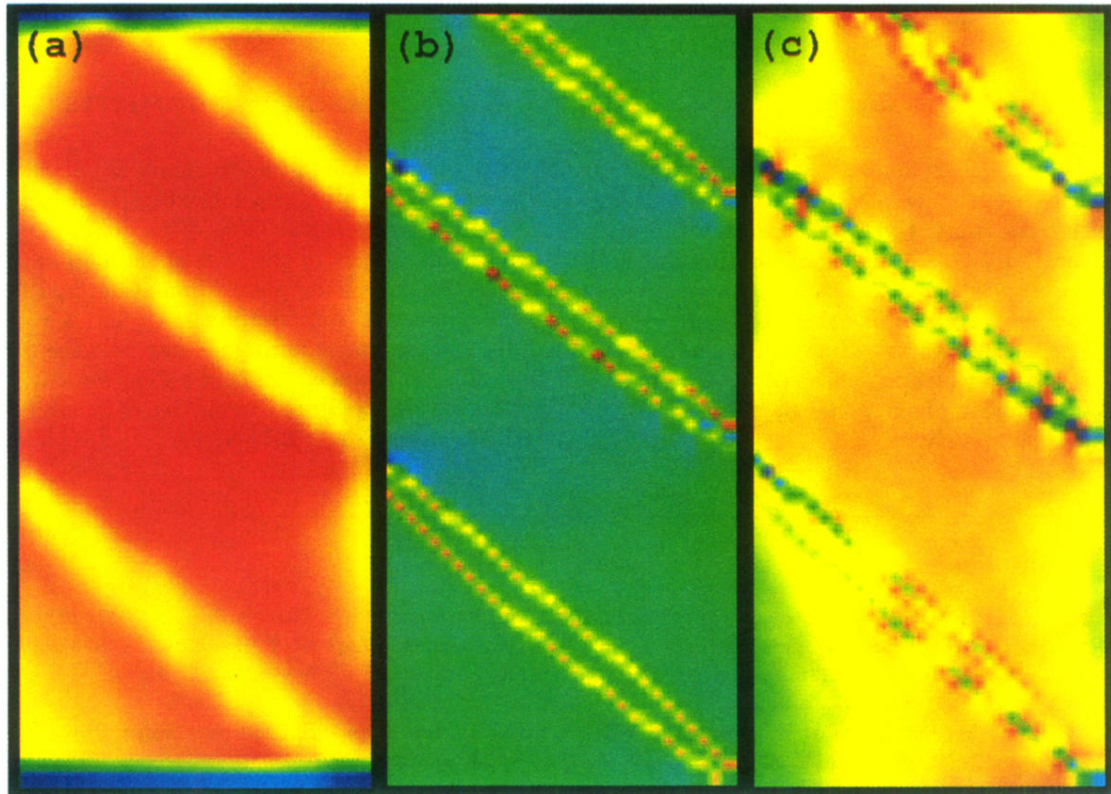


FIG. 10. The (a) smoothed spin, (b) YZ shear, and (c) ZZ deformation maps representing the initial particle configuration of the compressed crystal model before the commensurate $k = 0$ to incommensurate phase transition took place. The maps are drawn from the same state as the volume representations in Figs. 9(a) and 11(a). The Y and Z axes point to horizontal and vertical directions, respectively.

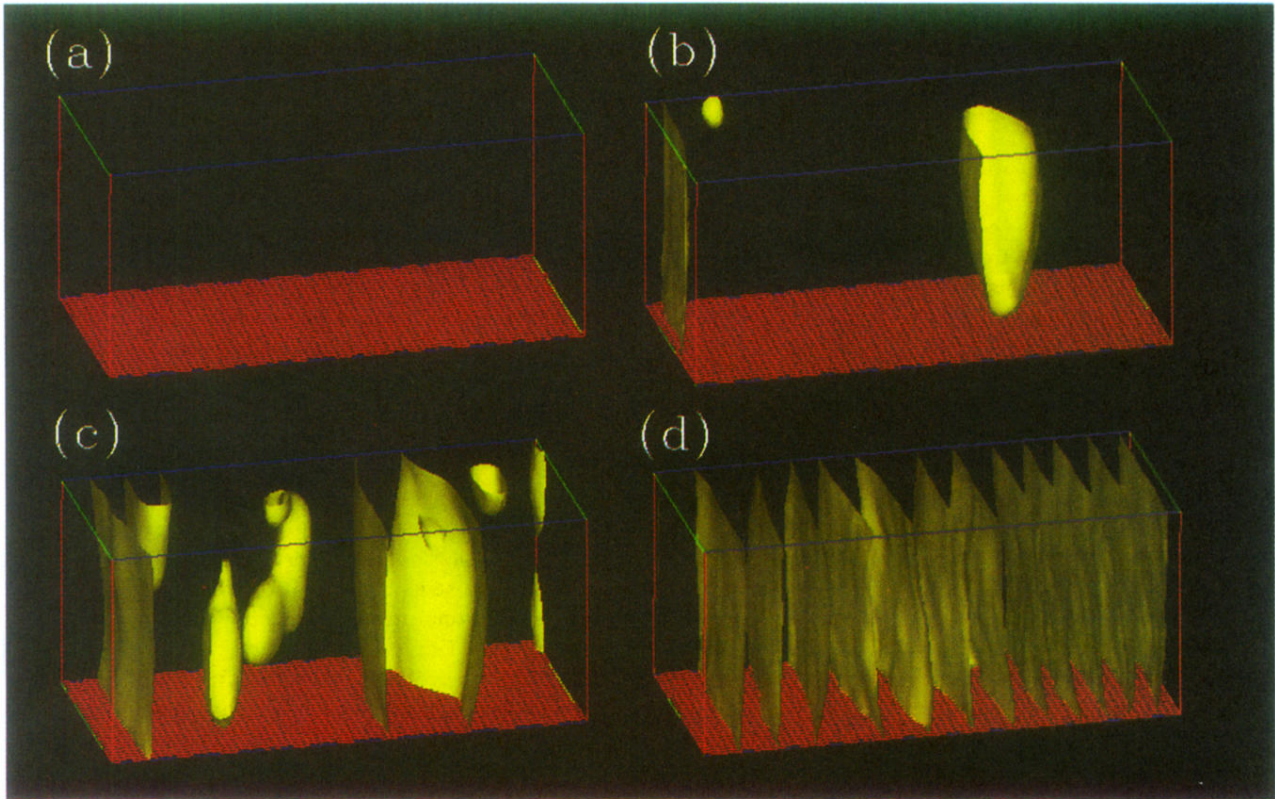


FIG. 11. Volume representation of the discommensuration planes (isosurface $D_{i,j,k} = 0$), showing four stages of the phase transition from commensurate $k = 0$ to incommensurate phase for the compressed crystal model. The X , Y and Z axes point to vertical, out of the figure plane, and horizontal directions of the crystallite, respectively.

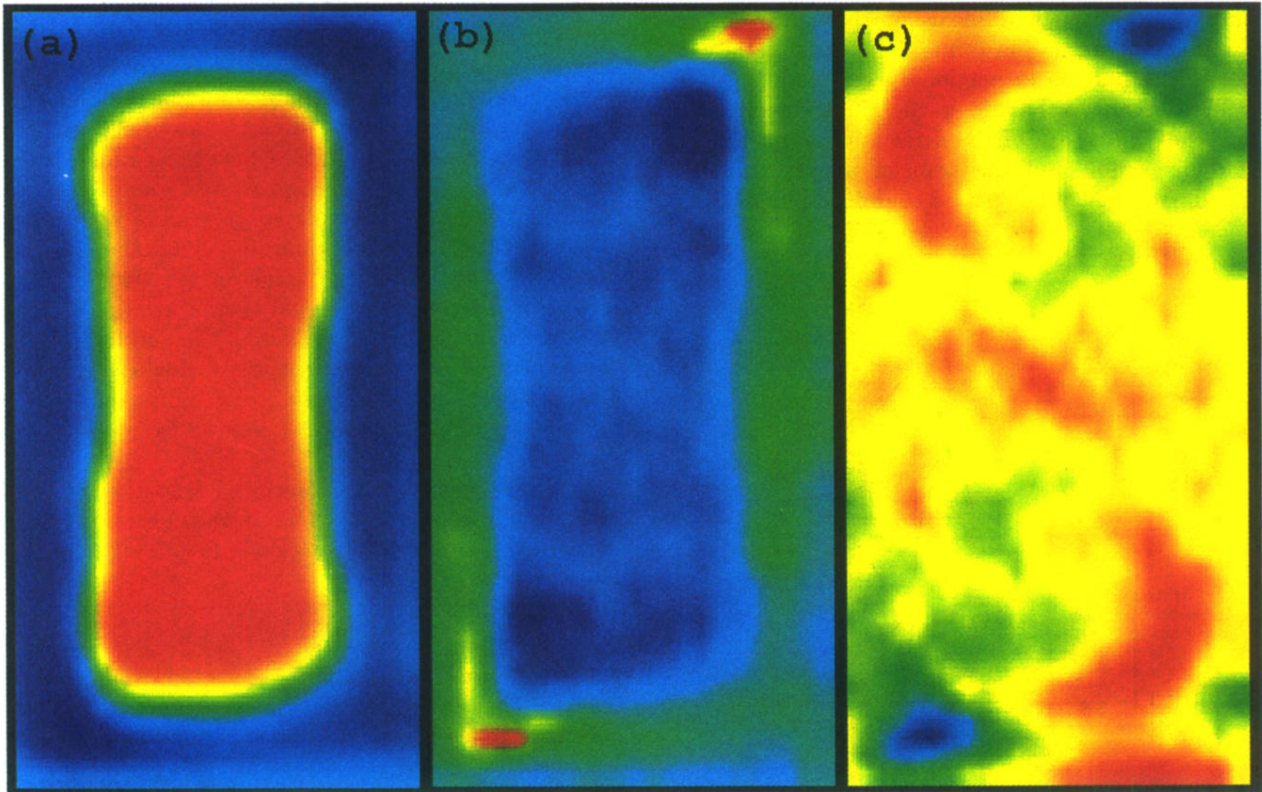


FIG. 2. The (a) smoothed spin, (b) YZ shear, and (c) ZZ deformation maps representing the initial particle configuration with the cylindrically shaped domain wall, before the commensurate $k = 0$ to incommensurate phase transition took place. The Y and Z axes point to horizontal and vertical directions, respectively.

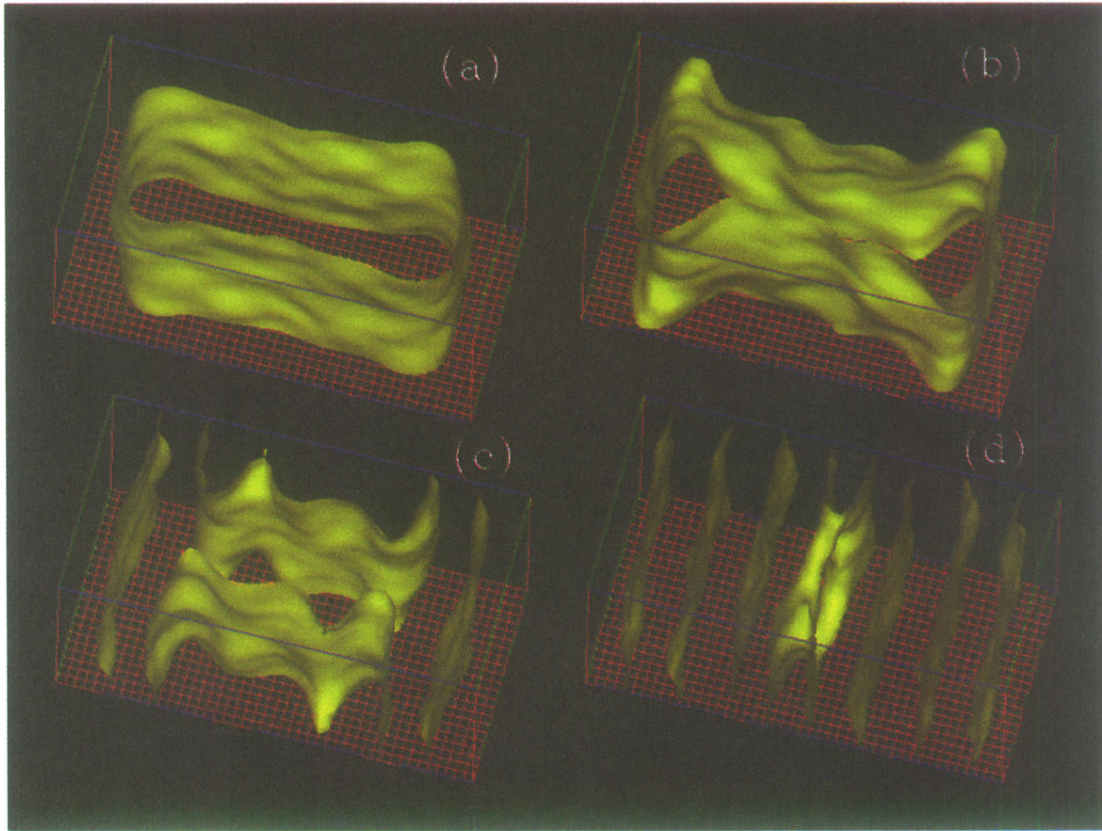


FIG. 4. Volume representation of the discommensuration planes (isosurface $D_{i,j,k} = 0$), showing four stages of the phase transition from commensurate $k = 0$ to incommensurate phase with initial domain pattern (a) in the form of a deformed cylinder. The particle configurations in (a) and (d) are the same as in the maps in Figs. 2 and 5, respectively. The X , Y , and Z axes point to vertical, out of the figure plane, and horizontal directions of the crystallite, respectively.

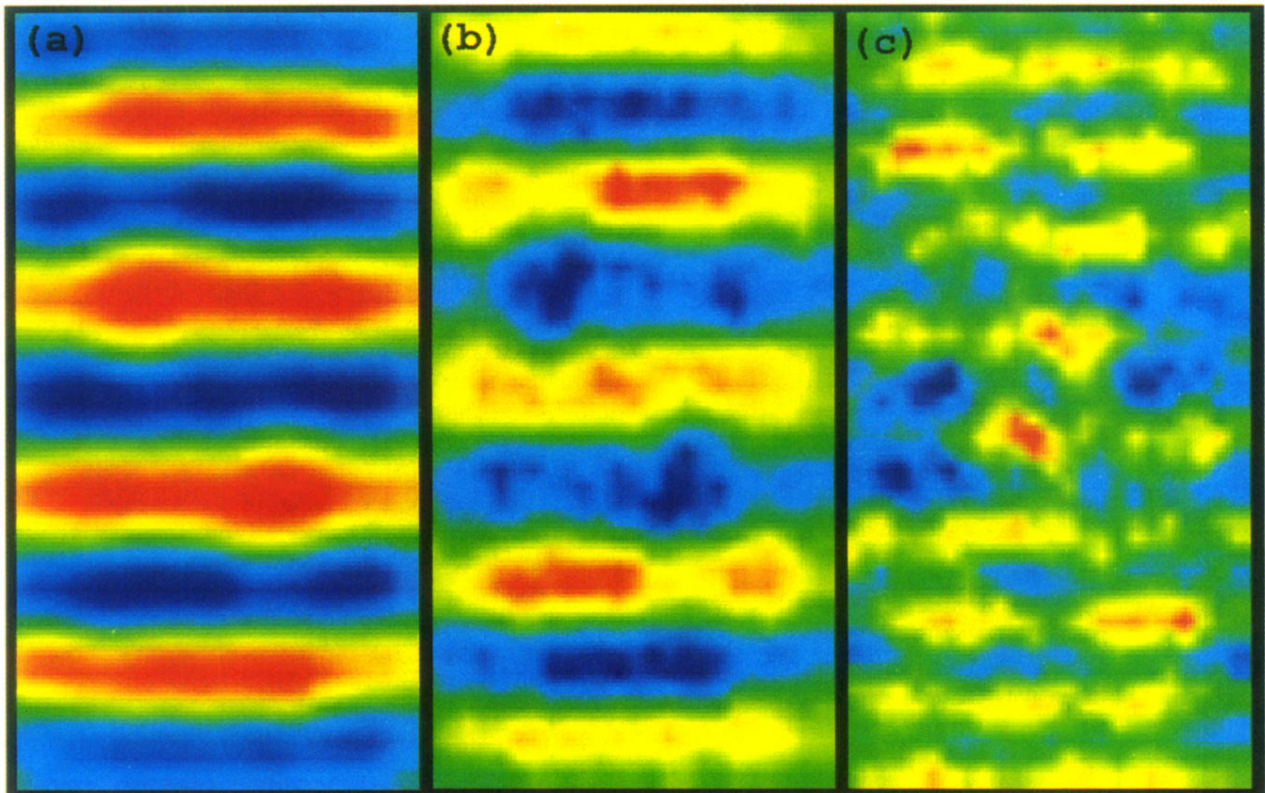


FIG. 5. The (a) smoothed spin, (b) YZ shear, and (c) ZZ deformation maps representing the final particle configuration after the phase transition from commensurate $k = 0$, with cylindrically shaped domain walls, to incommensurate phase took place. The Y and Z axes point to horizontal and vertical directions, respectively.

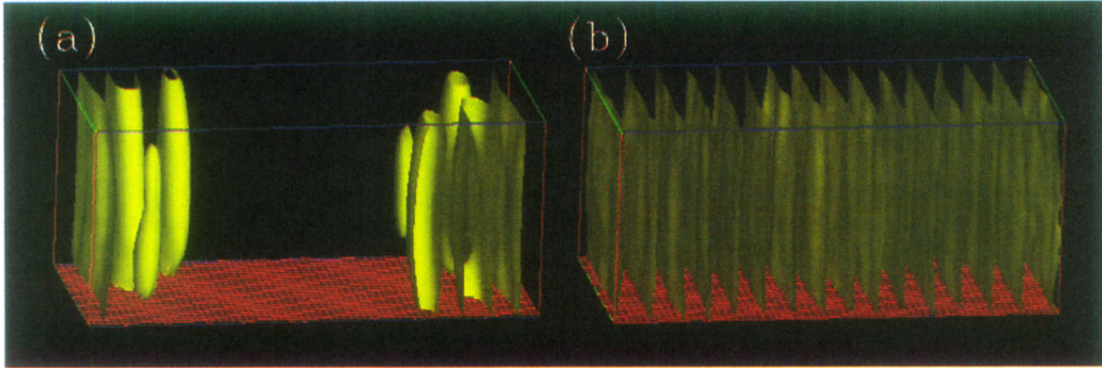


FIG. 7. Volume representation of the discommensuration planes (isosurface $D_{i,j,k} = 0$) taken (a) during phase transition from commensurate phase $k = 0$ to incommensurate phase, and (b) in the final incommensurate phase. The X , Y , and Z axes point to vertical, out of the figure plane, and horizontal directions of the crystallite, respectively.

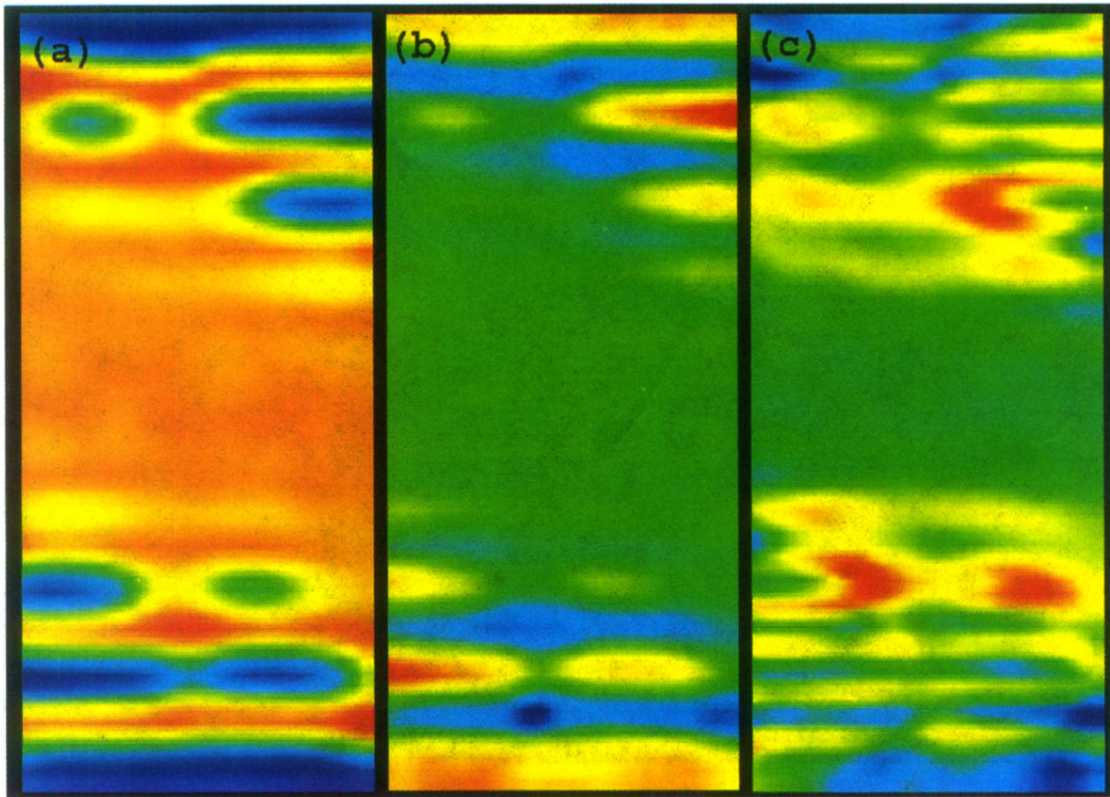


FIG. 8. The (a) smoothed spin, (b) YZ shear, and (c) ZZ deformation maps made during the phase transition from commensurate phase $k = 0$ to incommensurate phase. The particle configuration was the same as for Fig. 7(a). The Y and Z axes point to horizontal and vertical directions, respectively.

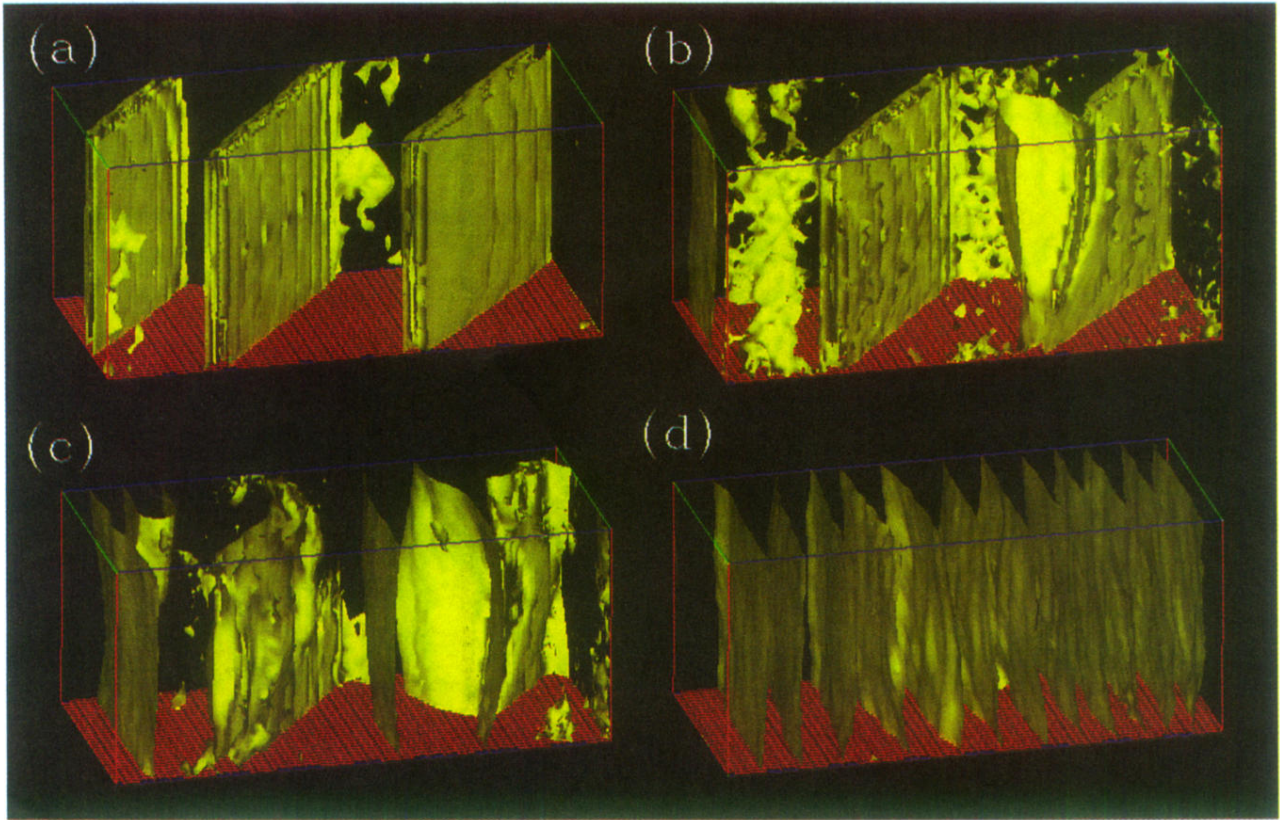


FIG. 9. Volume representation of the YZ shear component (isosurface $\sigma_{i,j,k}^{yz} = 0$), showing four stages of the phase transition from commensurate $k = 0$ to incommensurate phase for the compressed crystal model. The same states of the crystallite are drawn in Fig. 11 for the discommensuration planes. The X , Y and Z axes point to vertical, out of the figure plane, and horizontal directions of the crystallite, respectively.